



## Linear and Non-linear optical parameters of Copper Chloride doped Poly (Vinyl Alcohol) for Optoelectronic Applications

M. T. Ahmed<sup>1,2\*</sup>, A. Sarhan<sup>2</sup>, Z. M. Elqahtani<sup>3</sup>, W. B. Elsharkawy<sup>1</sup>, M. A Azzam<sup>4</sup>, T. Fahmy<sup>2</sup>

<sup>1</sup>Physics Department, College of Science and Humanities, Prince Sattam bin Abdulaziz University, 11942 Al-Kharj, Kingdom of Saudi Arabia. <sup>2</sup>Polymer Research Group, Physics Department, Faculty of Science, Mansoura University, 35516 Mansoura, Egypt. <sup>3</sup>Dept. of Physics, College of Science, Princess Nourah bint Abdulrahman University, Riyadh, Saudi Arabia <sup>4</sup>Chemistry Department, College of Science and Humanities, Prince Sattam bin Abdulaziz University, 11942 Al-Kharj, Kingdom of Saudi Arabia.



CrossMark

### Abstract

Poly (Vinyl Alcohol)/Copper Chloride (PVA/CuCl<sub>2</sub>) composite samples have been prepared using casting method with 1, 10 and 20 wt% of CuCl<sub>2</sub>. UV-Vis spectrum of these composites is investigated in the range of 200-900 nm. The absorption spectrum of PVA showed an absorption band at 278.18 nm and a small shoulder at 313.09 nm and are assigned to  $\pi$ - $\pi^*$  and  $n$ - $\pi^*$  transition, respectively. On the other hand, the spectra of the PVA/CuCl<sub>2</sub> composite samples showed a surface plasmon resonance (SPR) band in the visible band at 778.07 nm. Moreover, it is observed that, the absorption edge of composite samples is red shifted. Also, pure PVA showed an indirect and direct optical energy gap in the range of 4.71 and 5.08 eV, which decreased to 3.48 and 3.92 eV after CuCl<sub>2</sub> incorporation, indicating a structural defect in the matrix of PVA. It was also observed that nonlinear optical parameters such as third-order nonlinear optical sensitivity ( $\chi^{(3)}$ ) as well as the nonlinear refractive index ( $n_2$ ) are influenced by CuCl<sub>2</sub> incorporation and their values increased with increasing Cu chloride content. These results are very encouraging for possible applications in nonlinear optical (NLO) devices. The optical dielectric constant ( $\epsilon'$ ), dielectric loss ( $\epsilon''$ ) and photoconductivity have been investigated.

**Keywords:** PVA, Band gap, Urbach energy, Refractive index, Photoconductivity

### 1. Introduction

PVA is a linear organic polymer that possesses excellent optical properties, biocompatibility, biodegradability, and non-toxicity, and thus can be widely used in various applications [1-4]. PVA is water soluble, excellent optical transmission, non-corrosive and has good film-forming ability. These properties, especially their optical properties such as the energy gap and refractive index, enhance their industrial and technological uses in solar cell devices, optoelectronic materials, super capacitors, several types of sensors, ophthalmology and textile industry [5-6]. PVA is of great interest because it is relatively cheap, widely accessible, and has hydrophilic properties. The hydroxyl groups on the polyvinyl alcohol carbon backbone play an important role in creating the hydrogen bond between PVA and other substances, which in turn contributes to the formation of composites. PVA is an excellent host material, and so the structural, optical and electrical properties can be adapted

after incorporating different types of dopants into PVA [7-9].

A great deal of attention has been given to the study of doped polymers with different materials to obtain innovative multifunctional compounds for use in different applications. [10,11]. Polymer composites involve the strengthening and incorporation of dopant materials into the polymer matrix, resulting in enhanced electrical, optical and mechanical properties [12,13]. These properties are strongly influenced by various factors such as the nature of the polymer matrix, doping concentration, and the interaction between the polymer and doping materials [14,15]. Recently, studies on the electrical and optical properties of polymeric composites have greatly expanded in light of their wide applications in optical and electronic devices [16]. Polymer composites open new avenues for materials development to improve performance in many applications such as optical devices, coating materials, biosensors, and biomedical sciences

\*Corresponding author e-mail: [moustf\\_1@yahoo.com](mailto:moustf_1@yahoo.com)

Receive Date: 14 November 2021, Revise Date: 03 February 2022, Accept Date: 09 February 2022

DOI: 10.21608/EJCHEM.2022.105927.4878

©2022 National Information and Documentation Center (NIDOC)

[17,18]. Optoelectronic devices with excellent nonlinear optical properties are achieving technological importance due to daily inventions in the field of nanotechnology. Third-order nonlinearity is of paramount importance due to its potential applications in optical signal processing, optical switching, optical routers and ultra-fast nonlinear optical devices (NLO) [19].

Since the values of the optical bandgap and refractive index are taken into account when designing different optical devices, our aim in this manuscript is to prepare PVA/CuCl<sub>2</sub> composites. Moreover, the optical bandgap and refractive index as well as the dispersion-related parameters for PVA and PVA/CuCl<sub>2</sub> composites such as linear and nonlinear optical parameters will be studied and the obtained results will be analyzed.

## 2. Experimental Work

PVA (Mw= 72,000) and Copper Chloride (CuCl<sub>2</sub>) are supplied from Merck, (Germany) and BDH Chemicals Ltd, Poole, (England), respectively. Composite samples of PVA/CuCl<sub>2</sub> are prepared by dissolving PVA with a different ratio of copper chloride (1, 10 and 20 wt% of CuCl<sub>2</sub>) in double-distilled water (DDW) at T = 333 K for 10 h. The solution is constantly stirred for 6 hours using a hot plate with a magnetic stirrer to ensure that a homogeneous mixture is obtained. The solution is then poured into a Petri dish and dried in an oven for 1 day at T = 333 K. FTIR spectra have been recorded using FT-IR spectroscopy, Mattson in the range 4000 to 400 cm<sup>-1</sup>. UV-Vis spectra of PVA/CuCl<sub>2</sub> composite samples are carried out in the wavelength range from 200 to 900 nm by UV/VIS Unicam, Mattson, UK.

## 3. Results and Discussion

### 3.1: FTIR Spectroscopy

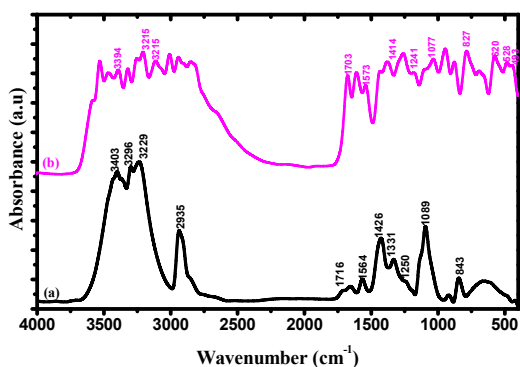


Fig. 1: FT-IR spectrum of pure and doped PVA/20 wt% CuCl<sub>2</sub> composites.

FTIR spectroscopy is used to examine the spectra of vibrations caused by differences in chemical compositions as well as changes in the functional group that occur during chemical reactions. FTIR studies give us valuable information about the interaction between the polymer and transition metals and the molecular structure. In the case of a chemical reaction, we observe a shift in the wave numbers and variation in the intensity of the peaks of some vibrational modes of the functional groups. Polymers can react with derivatives of transition metal ions or with each other to form a secondary bond, i.e., hydrogen bond [20]. Fig. 1 demonstrates the characteristic absorption bands of pure and doped PVA/CuCl<sub>2</sub> composite samples. FTIR spectrum of pure PVA showed several characteristic bands such as, 3403, 3296 and 3229 cm<sup>-1</sup> are assigned to O-H stretching confirming the existence of hydroxyl groups. These bands are shifted to lower wavenumber at 3394, 3215 and 3215 cm<sup>-1</sup>. The absorption band at 2935 cm<sup>-1</sup> is resulted from C-H stretching confirming the existence of methylene group [21]. The position of this band is shifted to higher wavenumber ~ at 2951 cm<sup>-1</sup> with increasing the content of CuCl<sub>2</sub> as observed in Fig. 1b. The stretching vibrational band of C=O is observed at 1716 cm<sup>-1</sup> and is attributed the carbonyl group due to the residual acetate group. It was also found that this band is shifted to a lower wavenumber with increasing CuCl<sub>2</sub> content and appeared at 1703 cm<sup>-1</sup>. The bands at 1564 and 1426 cm<sup>-1</sup> are assigned to C-H.

bending of CH<sub>2</sub> and -COO- stretching vibrations, respectively, while the absorption bands at 1331 and 1250 cm<sup>-1</sup> are related to the interaction between O-H bending and C-O stretching. The absorption band at 1089 cm<sup>-1</sup> is attributed to the C-O stretching vibration of the hydroxyl group and the intensity of this band is considered a measure of the crystallinity of PVA [22]. Obviously, the addition of CuCl<sub>2</sub> led to a decrease in the relative area and intensity of this band, as shown in Fig. 1b. Thus, these results supported the low degree of crystallinity of PVA and this will also be proven in the study and analysis of UV-Vis results that will be mentioned later. The strong band at 843 cm<sup>-1</sup> is due to the bending modes of CH<sub>2</sub> group. The weak absorption band at 493 cm<sup>-1</sup> is attributed to Cu-N bond [23].

Hence, the effect of CuCl<sub>2</sub> was demonstrated by the significant change in the intensity of the bands or by the shift of most absorption bands of the PVA films. These structural differences may be result from the

formation of crosslinking between oxygen atoms of the carbonyl groups and  $\text{Cu}^{2+}$  cation. This indicates that with increasing  $\text{Cu}^{2+}$  concentration the basicity of carbonyl groups will increase, which means that the  $\text{C}=\text{O}$  can act as a strong electron donor for the reaction with  $\text{Cu}^{2+}$ , leading to an increase in the

### 3.2: UV-Vis Spectroscopy

Fig. 2a displays the absorption spectrum of PVA and PVA/ $\text{CuCl}_2$  composite samples. It is found that, spectrum of PVA displayed an absorption band located at 278.18 nm and a small shoulder at 313.09 nm, respectively. The absorption band at 278.18 nm is related to the absorption of  $\text{C}=\text{O}$  groups conjugated with one ethylenic group of  $-\text{CO}-(\text{C}=\text{C})-$  and  $\text{CO}-(\text{C}=\text{C})_2-$ , while, the little shoulder at 313.09 nm is related to  $-\text{CO}-(\text{C}=\text{C})_3$ -groups [26,8]. These bands are assigned to  $\pi-\pi^*$  and  $n-\pi^*$  transition, respectively [27]. The region beyond 350 nm in the spectrum of PVA displayed a very low absorption and did not show any structure indicating that the PVA sample is

amorphous region of the PVA/ $\text{CuCl}_2$  composite samples [24]. Therefore, we can say that these structural differences indicate that the reaction between PVA and  $\text{CuCl}_2$  has taken place and therefore it plays an important role in improving the optical properties of the PVA/ $\text{CuCl}_2$  composites [25].

highly transparent in this region. On the other side, the spectrum of pure  $\text{CuCl}_2$  showed an absorption band at 236.84 nm. This band can be attributed to d-d transition of free  $\text{Cu}^{2+}$  [28]. The characteristic bands of pure  $\text{CuCl}_2$  and PVA have been shifted to appear at 251.76, 293.11 and 379.14 nm in PVA/ $\text{CuCl}_2$  composite samples, respectively. This means that  $\text{CuCl}_2$  interacted with PVA and modified the conformational and electronic structures. This shift in band position may be attributed to PVA/ $\text{Cu}$  complex formation. Moreover, a localized surface plasmon resonance (LSPR) band is obtained in the visible region at  $\sim 778.07$  nm of the spectrum of PVA/ $\text{CuCl}_2$

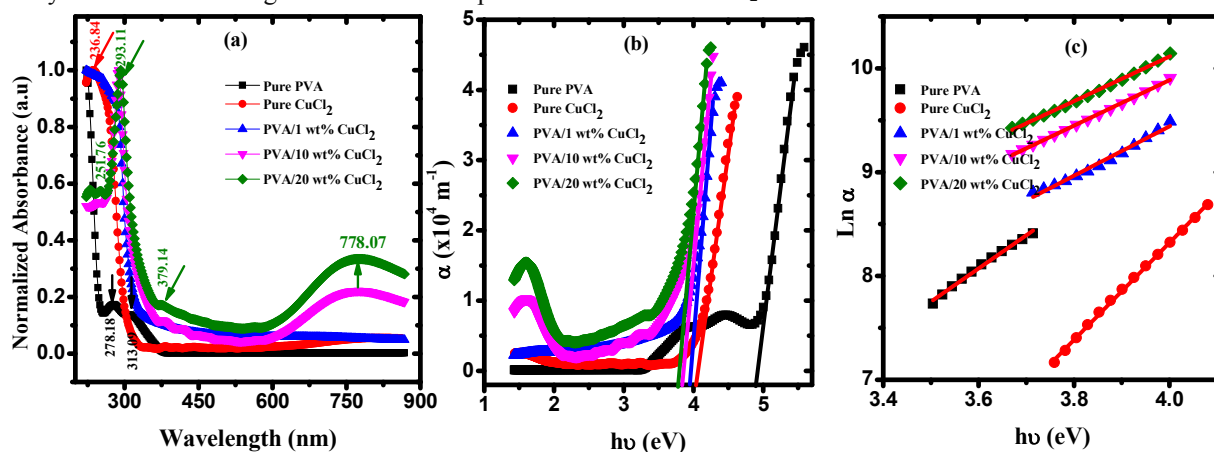


Fig. 2: a) Absorbance against wavelength, b) Absorption coefficient against  $h\nu$  and (c)  $\ln \alpha$  against  $h\nu$  of pure PVA and PVA/ $\text{CuCl}_2$  composite samples.

composite samples. In the visible wavelength region, the LSPR differs for different metallic particles due to the different dielectric properties that arose from the small overlap between interband transition and the LSPR. Cu has a completely filled 3D orbital and only one electron in 4s orbital. The interband transition takes place in the broad conduction band, thus the LSPR peak is very wide and the interband transitions overlap with the LSPR. This results in an increase in the width of the LSPR as well as a decrease in the intensity of the LSPR. The properties of the resonance depend on the particles and dispersing medium properties because they polarize each other, and the charge density must adapt not only to the incident fields but also to the field induced by the polarization [29]. The absorption coefficient ( $\alpha$ ) is estimated based on the following formula

$$\alpha = 2.303 \frac{A}{d} \quad (1)$$

Where  $A$  is the absorbance and  $d$  is sample thickness, respectively. Fig. 2b displays the

absorption coefficient behavior versus the photon energy ( $h\nu$ ). The redshift of absorption edge observed in Fig. 2b confirms the optical bandgap change of the PVA films after doping with  $\text{CuCl}_2$ . The values of absorption edge are estimated by extrapolating the linear plot to  $\alpha = 0$  at the linear region as shown in Fig. 1b and summarized in Table 1. It is observed that the absorption edge decreases with increasing  $\text{CuCl}_2$  content in the PVA matrix. The absorption data can be used to calculate Urbach energy ( $E_U$ ). The exponential dependence of the absorption coefficient ( $\alpha$ ) on the photon energy ( $h\nu$ ) is expressed according to Urbach equation as follows [30]

$$\alpha = \alpha_0 \exp\left(\frac{h\nu}{E_U}\right) \quad (2)$$

Where  $\alpha_0$  is the pre-exponential factor and  $E_U$  is the width of the band tail, respectively. In many semi-crystalline and amorphous materials, the exponential dependence of the absorption coefficient ( $\alpha$ ) on the photon energy arises from random fluctuations in the internal fields which correlate with

the structural disorder. Urbach energy ( $E_U$ ) may be assumed to be a parameter that contains the effects of all possible defects and depends on structural disorder degree. Fig. 1c displays a linear relationship between  $\ln \alpha$  and  $h\nu$  for all samples under investigation. By knowing the slope of the linear fit of Fig. 2c,  $E_U$  values are calculated and tabulated in Table 1. Urbach energy values were found to increase with increasing  $\text{CuCl}_2$  content. The increased tail width can be explained by the fact that an increase in  $\text{CuCl}_2$  content may lead to defects and imperfections in the semicrystalline structure of PVA/ $\text{CuCl}_2$  composite samples, a condition that may increase localized states within the forbidden energy bandgap. This behavior is in good agreement with previously published works of polymer composite or polymer blend systems [9,31,32]. The steepness parameter ( $\beta$ ), which is a measure of the optical absorption edge broadening caused by the interaction of exciton-phonon or electron-phonon can be estimated using  $E_U$  values as follow

$$\beta = \frac{k_B T}{E_U} \quad (3)$$

where  $k_B$  is the Boltzmann constant and  $T$  is the temperature, respectively. The  $\beta$  values are estimated at  $T=300$  K and summarized in Table 1.

The optical band gap is an essential parameter for photonic, electronic, optical-electronic devices and designing solar cell. The electronic transitions of PVA/ $\text{CuCl}_2$  composites are determined by investigating the optical bandgap energy using the following equation [33]

$$(\alpha h\nu)^{1/m} = B(h\nu - E_g) \quad (4)$$

Where  $B$ ,  $h\nu$  and  $E_g$  are constant, photon energy, the optical bandgap energy and  $m$  is a constant for direct and indirect allowed transitions equals to  $1/2$  and 2, while, equals  $3/2$  and 3 for direct and indirect forbidden transitions, respectively. Indirect and direct optical bandgap energy values of PVA/ $\text{CuCl}_2$  composite samples can be evaluated by extrapolation of the plot of  $(\alpha h\nu)^{1/2}$  and  $(\alpha h\nu)^2$  against  $h\nu$ , as illustrated in Fig. 3(a&b).

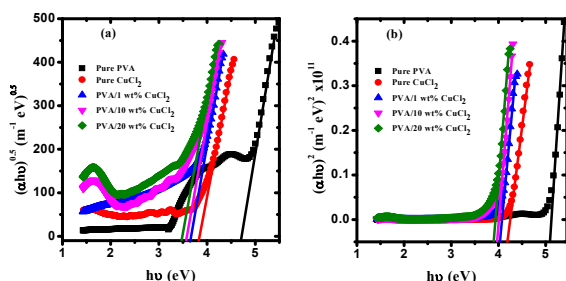


Fig. 3: a)  $(\alpha h\nu)^{0.5}$  b)  $(\alpha h\nu)^2$  versus  $h\nu$  of pure PVA and PVA/ $\text{CuCl}_2$  composite samples.

By extrapolating the linear plot to  $(\alpha h\nu)^{0.5}$  and  $(\alpha h\nu)^2 = 0$  at the linear region as illustrated in Fig. 3,

the values of indirect and direct optical bandgap of PVA/ $\text{CuCl}_2$  composite samples are calculated and tabulated in Table 1. We observed that, both direct and indirect optical bandgap energies are decreased with the increase of  $\text{CuCl}_2$  in the PVA matrix as a result of the polymer structure disorder due to the presence of  $\text{CuCl}_2$ . This structure disorder leads to localized states formation in the forbidden bandgap of the PVA host matrix. These states are allowed to release and trap electrons between the valence band and conduction band [34]. The variation in optical bandgap energy values ( $E_g$ ) of the composite films confirmed the modification of PVA microstructure as well as the band structure, which might be due to the creation of additional clusters of optical transitions. The lower bandgap also confirms the increased disorder degree in the polymer composite samples. These results are quite consistent with the bandwidth values of the localized tail states in the forbidden bandgap as mentioned above, i.e., Urbach energy ( $E_U$ ). The lower energy gap value of PVA after incorporation of  $\text{CuCl}_2$  makes it highly candidates to be effective materials for optoelectronic devices. This is because such devices require bandgap tuning.

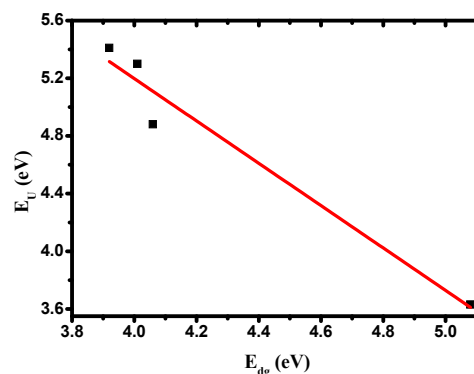


Fig. 4: Urbach energy versus direct optical bandgap energy.

Fig. 4 displays the variation of the direct optical energy gap versus Urbach energy. One can conclude that an increase in the Urbach energy of the material gives an indication of the decrease in the values of optical energy gap. This observation supports that by incorporating  $\text{CuCl}_2$  the number of traps will increase. The carbon atoms ( $M$ ) per each cluster in the samples of PVA/ $\text{CuCl}_2$  composites can be calculated using the direct optical bandgap values by the following equation [35]:

$$E_{dg} = \frac{34.3}{\sqrt{M}} \quad (5)$$

The values of carbon atoms have been estimated and summarized in Table 1. It is observed that the  $M$  value of pure PVA, which is about 46 is increased to 77 in PVA/20 wt%  $\text{CuCl}_2$ . This increase can be related to the increased conjugation of the monomer units in PVA after doping with  $\text{CuCl}_2$  [36].

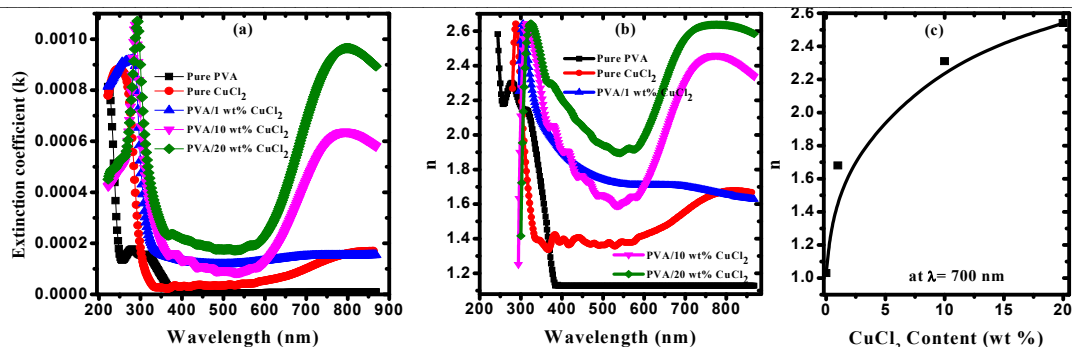


Fig. 5: a) The extinction coefficient versus wavelength b) refractive index (n) versus wavelength and c) refractive index (n) versus CuCl<sub>2</sub> content

Materials optical characterization is generally governed to the interaction between the materials and the electric field of incident electromagnetic wave. The absorption coefficient ( $\alpha$ ) is used to calculate the extinction coefficient ( $k$ ) values according to the following equation

$$k = \frac{\alpha\lambda}{4\pi} \quad (6)$$

The dependence of extinction coefficient and refractive index on the incident light wavelength for PVA/CuCl<sub>2</sub> composite samples is depicted in Fig. 5(a&b). It is found that the extinction coefficient ( $k$ ) decreases with increasing wavelength in UV region, while the values of  $k$  start to increase with increasing wavelength again in the visible region (~ 400-900 nm) as well as with increasing concentration of CuCl<sub>2</sub>. The incident photons in the UV region have a high enough energy to excite electrons to overcome the bandgap and thus, the values of  $k$  decrease. The decrease in  $k$  values confirms that the electromagnetic waves are allowed to pass in this region without any damping or decay through these composites. In contrast, in the visible light region, the energy of the photon cannot excite the electrons from one state to another one, so this energy will be lost due to reflection or scattering, which leads to an increase in the values of  $k$  in this region [34].

The refractive index control of polymeric materials makes them suitable for numerous industrial and medical applications such as organic solar cell, anti-reflective coatings, LEDs, optical communications, and polymeric lenses. The refractive index ( $n$ ) is estimated using the values of reflectance ( $R$ ) according to the following relation,

$$n = \frac{1 + \sqrt{R}}{1 - \sqrt{R}}, \text{ where } R = 1 - \sqrt{T \exp(A)}, \text{ where } T$$

and  $A$  are the transmittance and the absorbance, respectively [37]. Fig. 4b depicts the wavelength dependence of the refractive index ( $n$ ). It was found that the refractive index of all samples are decreased with increasing wavelength to approximately 500 nm, while in the range from 550 to 950 nm it almost does not change with the wavelength for pure PVA while it increases again for PVA/CuCl<sub>2</sub> composite samples. Also, the refractive index of pure PVA in the visible region at 700 nm is increased from 1.03 to

2.54 (for higher concentration 20 wt% CuCl<sub>2</sub>). Fig. 5c revealed that the refractive index is increased nonlinearly with increasing concentration of CuCl<sub>2</sub>. The increase in the refractive index with increasing CuCl<sub>2</sub> content in PVA host matrix can be related to an increase of the free charge carrier concentration and in the reflectivity of the polymer samples [38].

Refractive index of our investigated PVA/CuCl<sub>2</sub> composite samples is analyzed by the single-oscillator model [37] as follow:

$$n^2 = 1 + \frac{E_d E_o}{E_o^2 - (h\nu)^2}$$

$$(n^2 - 1)^{-1} = \frac{E_o}{E_d} - \frac{(h\nu)^2}{E_o E_d} \quad (7)$$

Where  $E_d$  is the dispersion energy that measures the strength of the oscillator and  $E_o$  is the energy of single oscillator of the electronic transition, respectively. Fig. 6 displays the variation of  $(n^2 - 1)^{-1}$  against  $(h\nu)^2$  for all samples. By knowing the values of both intercept and slope of Eq. (7), the values of  $E_o$  and  $E_d$  are evaluated and summarized in Table 1.

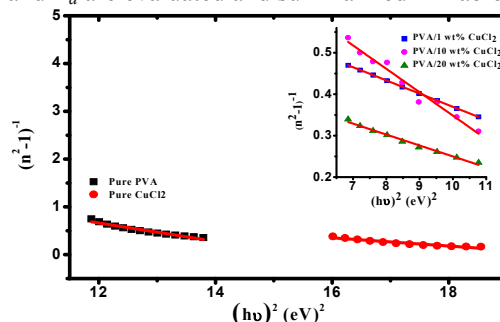


Fig. 6:  $(n^2 - 1)^{-1}$  versus  $(h\nu)^2$  of pure PVA and PVA/CuCl<sub>2</sub> composite samples.

The optical spectrum moments ( $M_{-1}$  and  $M_{-3}$ ) which measures the process of light-material interaction are calculated by using the oscillator parameters as follows [37]:

$$E_o^2 = \frac{M_{-1}}{M_{-3}} \text{ and } E_d^2 = \frac{M^3}{M_{-3}} \quad (8a)$$

Rearranging the previous Eq. (8a), the values  $M_{-1}$  and  $M_{-3}$  for the investigated PVA/CuCl<sub>2</sub> composite samples can be calculated as follows:

$$M_{-1} = \frac{E_d}{E_0} \quad \text{and} \quad M_{-3} = \frac{M_{-1}}{E_0^2} \quad (8b)$$

$M_{-1}$  and  $M_{-3}$  values all samples are estimated and summarized in Table 1 and it is found that the values of  $M_{-1}$  and  $M_{-3}$  are increased with increasing  $\text{CuCl}_2$  content. In addition, the zero-frequency refractive index, i.e., static refractive index ( $n_0$ ) of our studied samples is determined using the following relationship:

$$n_0 = \left(1 + \frac{E_d}{E_0}\right)^{0.5} \quad (9)$$

Thus, the static dielectric constant ( $\epsilon_s$ ) can be estimated using values of linear static refractive index ( $n_0$ ) for all samples according to the following formula,

$$\epsilon_s = n_0^2 \quad (10)$$

Optical oscillator strength ( $f$ ) for the optical transmission which refers to the photon absorption process by the electron between the initial and final states and is also related to  $E_0$  and  $E_d$  as follows,  $f = E_0 E_d$  has been estimated and tabulated in Table 1. The results revealed that the values of  $n_0$ ,  $\epsilon_s$  and  $f$  are increased with increasing the concentration of  $\text{CuCl}_2$ . This increase in refractive index enhances the potential for these composites to be used in a wide range of applications from anti-reflective coatings of solar cell devices to high refractive index lenses.

The correlation between ( $n^2$ ) and ( $\lambda^2$ ) is used to calculate the values of the lattice dielectric constant ( $\epsilon_L$ ), as follows [37]:

$$n^2 = \epsilon_L - \frac{e^2}{4\pi\epsilon_0 c^2} \left(\frac{N}{m^*}\right) \lambda^2 \quad (11)$$

where  $e$ ,  $\epsilon_0$ ,  $c$  and ( $N/m^*$ ) are electronic charge, free space permittivity ( $8.854 \times 10^{-12}$  F/m), light speed and ratio of carrier concentration to effective mass, respectively. Fig. 7a illustrates the dependence of  $n^2$  on  $\lambda^2$  for all samples. The values of lattice dielectric constant ( $\epsilon_L$ ) and ( $N/m^*$ ) are calculated by knowing the intercept and slope of Fig. 7a and summarized in Table 1. The results in Table 1 showed that, the values of lattice dielectric constant ( $\epsilon_L$ ) are higher than the values of static dielectric constant ( $\epsilon_s$ ). This difference can be attributed to the contribution of the polarization process that occurs inside the material when light falls on it as well as the increase in the concentration of the free carriers. Also, as is evident from Table 1 that  $E_0$ ,  $E_d$ ,  $n_0$  and  $\epsilon_s$  values are increased with increasing  $\text{CuCl}_2$  content in PVA host matrix. This indicates an increase in the degree of disorder in the PVA structure as well as an increase in charge transfer between PVA macromolecules and  $\text{CuCl}_2$  [39].

The plasma frequency ( $\omega_p$ ) values of PVA/ $\text{CuCl}_2$  composite samples are calculated using the values of ( $N/m^*$ ) and summarized in Table 1, according to the following equation:

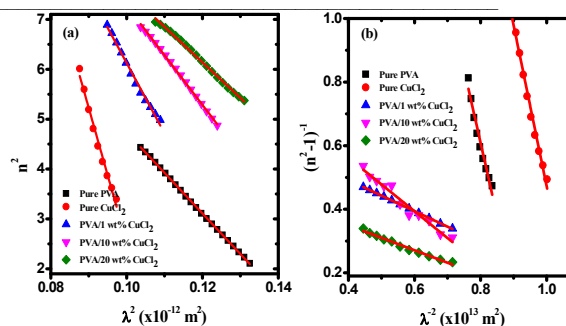


Fig. 7: a)  $n^2$  versus  $\lambda^2$  and b)  $(n^2-1)^{-1}$  versus  $\lambda^2$ .

$$\omega_p^2 = \frac{e^2}{\epsilon_0} \left(\frac{N}{m^*}\right) \quad (12)$$

Where,  $\epsilon_0$  is the permittivity constant ( $\epsilon_0 = 8.854 \times 10^{-12}$  F  $\text{m}^{-1}$ ). The high values of plasma frequency are attributed to high values of free carrier concentrations.

To estimate the static optical refractive index ( $n_0$ ) at an infinite wavelength, the Wemple-Didomenico formula has been modified as follows [40]:

$$\frac{n_0^2 - 1}{n^2 - 1} = 1 - \left(\frac{\lambda_0}{\lambda}\right)^2 \quad (13)$$

Where  $\lambda_0$  is the average oscillator wavelength.

$$\frac{n_0^2 - 1}{n^2 - 1} = \frac{\lambda^2 - \lambda_0^2}{\lambda^2} \quad (14)$$

The dispersion equation in Eq. (7) can be rewritten in terms of  $\lambda$  by using  $E = hc/\lambda$ , as follows:

$$(n^2 - 1)^{-1} = \frac{E_0}{E_d} - \frac{(hc)^2}{E_0 E_d} \frac{1}{\lambda^2} \quad (15)$$

Hence, from the comparison between Eq. (14) and Eq. (15), we can deduce that:

$$\frac{E_0}{E_d} = \frac{1}{n_0^2 - 1} \quad \text{and} \quad \frac{h^2 c^2}{E_0 E_d} = \frac{\lambda_0^2}{n_0^2 - 1} \quad (16)$$

Therefore, from Eq. (16), we can deduce that:

$$E_0 = \frac{hc}{\lambda_0} \quad \text{and} \quad E_d = \frac{hc(n_0^2 - 1)}{\lambda_0} \quad (17)$$

Thus Eq. (14) can be rewritten in terms average oscillator wavelength ( $\lambda_0$ ) and of average oscillator strength ( $s_0$ ) as follows:

$$n^2 - 1 = \frac{s_0 \lambda_0^2}{1 - \left(\frac{\lambda_0}{\lambda}\right)^2} = \frac{s_0 \lambda_0^2 \lambda^2}{\lambda^2 - \lambda_0^2} \quad (18)$$

$$\text{Where, } s_0 = \frac{(n_0^2 - 1)}{\lambda_0^2}$$

So, the values of ( $s_0$ ) and ( $\lambda_0$ ) can be estimated by using the values of  $E_0$  and  $n_0$  or experimentally by plotting  $(n^2-1)^{-1}$  versus  $\lambda^{-2}$  based on the Eq.(18), as shown in Fig. 7b. By knowing the slope and intercept of Fig. 7b, the values of  $s_0$  and  $\lambda_0$  are calculated and summarized in Table 1. It was found that the values of  $s_0$  and  $\lambda_0$  that are calculated in different ways are matching to each other.

### 3.2: Nonlinear optical parameters

From applications towards photonics, optical switching and self-focusing, investigation of nonlinear optical (NLO) parameters such as susceptibility and refractive index is essential and required. When an optical field is applied to the material, the material is polarized, and then nonlinearity occurs. Third-order nonlinear optical susceptibility,  $\chi^{(3)}$  and nonlinear refractive index ( $n_2$ ) are taken into consideration as a very important nonlinear optical parameters for many applications such as, systems of capacitive communication [41].

According to Miller's rule,  $\chi^{(3)}$  can be estimated using the following equation [42]

$$\chi^{(3)} = A(\chi^{(1)})^4 \quad (19)$$

Where  $A$  is a constant and equals to  $1.79 \times 10^{-10}$  esu and  $\chi^{(1)}$  is the linear optical susceptibility and given by

$$\chi^{(1)} = E_d / 4\pi E_0 \quad (20)$$

Hence,  $\chi^{(3)}$  can be expressed in the form of

$$\begin{aligned} \chi^{(3)} &= A \left( \frac{E_d}{4\pi E_0} \right)^4 \\ &= \frac{A}{(4\pi)^4} (n_0^2 - 1)^4 \end{aligned} \quad (21)$$

The values of ( $n_2$ ) are estimated using the values of ( $n_0$ ) and ( $\chi^{(3)}$ ) based on Miller's rule as follow: [43]

$$n_2 = \frac{12\pi}{n_0} \chi^{(3)} \quad (22)$$

The values of linear and non-linear optical parameters ( $\chi^{(1)}$ ,  $\chi^{(3)}$ ,  $n_2$ ) of all samples are estimated and listed in Table 1. High values of  $n_2$  indicate that the studied PVA/CuCl<sub>2</sub> composite samples could be interesting candidates for nonlinear optical applications.

Table 1: The optical parameters values of PVA/CuCl<sub>2</sub> composite samples.

	Pure PVA	CuCl <sub>2</sub>	PVA/1 wt% CuCl <sub>2</sub>	PVA/10 wt% CuCl <sub>2</sub>	PVA/20 wt% CuCl <sub>2</sub>
Absorption edge, (eV)	4.88	3.99	3.87	3.77	3.69
Urbach tail, (eV)	3.629	2.484	4.884	5.301	5.412
Steepness parameter, ( $\beta$ )	0.0071	0.0104	0.0052	0.0048	0.0047
Indirect bandgap energy, (eV)	4.71	3.83	3.65	3.56	3.48
Direct bandgap energy, (eV)	5.08	4.20	4.06	4.01	3.92
Carbon atoms (M)	46	--	71	73	77
Lattice dielectric constant, $\epsilon_L$	12.86	29.51	20.21	17.22	14.68
$N/m^*$ ( $m^{-3} kg^{-1}$ )	$9.97 \times 10^{58}$	$3.31 \times 10^{59}$	$1.72 \times 10^{59}$	$1.22 \times 10^{59}$	$8.74 \times 10^{58}$
Plasma frequency, $\omega_p$ (Hz)	$1.69 \times 10^{16}$	$3.09 \times 10^{16}$	$2.23 \times 10^{16}$	$1.87 \times 10^{16}$	$1.59 \times 10^{16}$
Oscillator energy ( $E_0$ ), (eV)	3.93	4.49	4.78	4.27	5.06
Dispersion energy ( $E_d$ ), (eV)	1.32	2.62	6.96	4.68	9.87
$M_1$	0.580	0.762	1.205	1.047	1.396
$M_3$ , (eV) <sup>-2</sup>	0.037	0.037	0.052	0.057	0.054
Static refractive index ( $n_0$ )	0.668	0.791	1.226	1.048	1.474
Static dielectric constant ( $\epsilon_s$ )	1.336	1.581	2.453	2.096	2.949
Optical oscillator strength ( $f$ ) (eV) <sup>2</sup>	5.208	11.764	33.333	20	50
*Average single oscillator wavelength ( $\lambda_0$ ) (m)	$3.15 \times 10^{-7}$	$2.75 \times 10^{-7}$	$2.59 \times 10^{-7}$	$2.90 \times 10^{-7}$	$2.45 \times 10^{-7}$
*Average single oscillator strength ( $s_0$ ) (m <sup>-2</sup> )	$3.38 \times 10^{12}$	$7.64 \times 10^{12}$	$2.16 \times 10^{13}$	$1.29 \times 10^{13}$	$3.24 \times 10^{13}$
**Average single oscillator wavelength ( $\lambda_0$ ) (m)	$3.27 \times 10^{-7}$	$3.02 \times 10^{-7}$	$2.66 \times 10^{-7}$	$3.06 \times 10^{-7}$	$2.78 \times 10^{-7}$
**Average single oscillator strength ( $s_0$ ) (m <sup>-2</sup> )	$2.16 \times 10^{12}$	$1.98 \times 10^{12}$	$2.05 \times 10^{13}$	$1.19 \times 10^{13}$	$2.55 \times 10^{13}$
Linear optical susceptibility $\chi^{(1)}$	$2.68 \times 10^{-2}$	$4.62 \times 10^{-2}$	$11.57 \times 10^{-2}$	$8.73 \times 10^{-2}$	$15.52 \times 10^{-2}$
Third-order nonlinear optical susceptibility $\chi^{(3)}$ (e.s.u.)	$9.24 \times 10^{-17}$	$8.21 \times 10^{-16}$	$3.21 \times 10^{-14}$	$1.04 \times 10^{-14}$	$1.03 \times 10^{-13}$
Nonlinear refractive index ( $n_2$ ) (e.s.u.)	$5.21 \times 10^{-15}$	$3.91 \times 10^{-14}$	$9.86 \times 10^{-13}$	$3.73 \times 10^{-13}$	$2.65 \times 10^{-12}$

\*) The values of  $s_0$  and  $\lambda_0$  are calculated using the values of  $E_0$  and  $n_0$ .

\*\*\*) The values of  $s_0$  and  $\lambda_0$  are calculated experimentally from  $(n^2-1)^{-1}$  vs  $\lambda^2$ .

### 3.3: Optical dielectric constant and optical conductivity

The materials polarizability is related to the dielectric constants. The real ( $\epsilon'$ ) and imaginary ( $\epsilon''$ ), (which are useful to understand the capacitive/resistive nature of material) parts of its complex ( $\epsilon^*$ ) can be expressed as:  $\epsilon^* = \epsilon' + i\epsilon''$ .  $\epsilon'$  and  $\epsilon''$  parts of the optical dielectric constant depend on the refractive index ( $n$ ) and extinction coefficient ( $k$ ) values and can be determined as:  $\epsilon' = n^2 - k^2$ , whereas,  $\epsilon'' = 2nk$ . Fig. 8(a&b) illustrated the variation of ( $\epsilon'$ ) and ( $\epsilon''$ ) versus the incident wavelength for all samples. It is found that,  $\epsilon'$  and  $\epsilon''$  have the same trend but values of  $\epsilon'$  are larger than of  $\epsilon''$ . This difference in the values of  $\epsilon'$  and  $\epsilon''$

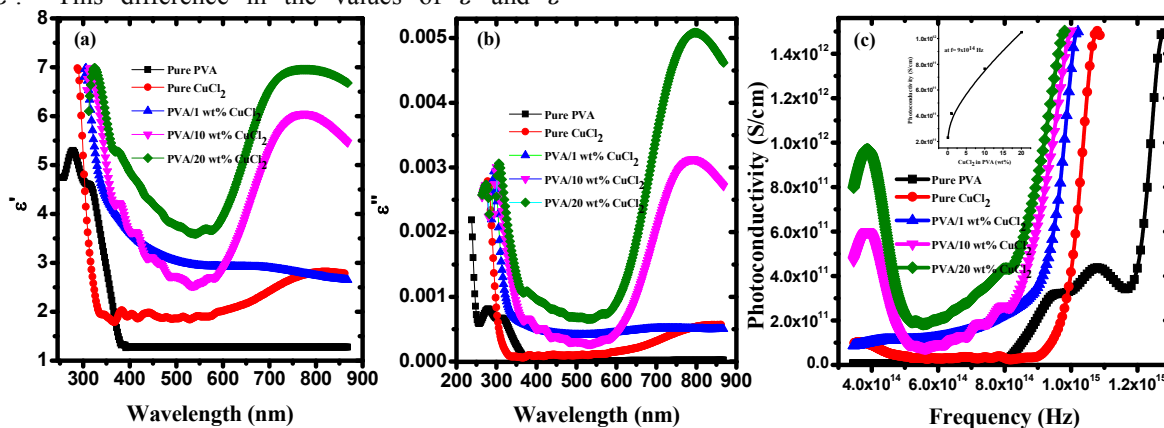


Fig. 8:

a) dielectric constant against wavelength, b) dielectric loss against wavelength and c) Photoconductivity against frequency of pure PVA/CuCl<sub>2</sub> composite samples.

The optical conductivity ( $\sigma_{op}$ ) is estimated using the formula,  $\sigma_{op} = nca/4\pi$ . Fig. 8c displays the variation of optical conductivity of PVA/CuCl<sub>2</sub> composite samples versus wavelength. It is found that optical conductivity increases with increasing frequency and CuCl<sub>2</sub> content in the PVA matrix. The increase in the optical conductivity indicates that concentration of charge carriers in the PVA/CuCl<sub>2</sub> composite samples is increased. On the other hand, the lower values of optical conductivity at lower frequency may be due to the less availability of mobile charge carriers to transport from one localized state to another because of the interfacial polarization (IP) effect [46,47]. On the other hand, as the frequency increases, the average charge carrier displacement decreases and therefore the conductivity will increase.

### 4. Conclusion

UV-Vis spectrum of pure PVA and PVA/CuCl<sub>2</sub> composite samples displayed that, pure PVA is characterized by an absorption band at 278.18 nm and a little shoulder at 313.09 nm. These bands are assigned to  $\pi-\pi^*$  and  $n-\pi^*$  transition, respectively. The absorption band of pure CuCl<sub>2</sub> is observed at 236.84 nm and attributed to d-d transition of free Cu<sup>2+</sup>. The bands of pure PVA and CuCl<sub>2</sub> are observed at higher wavelengths in PVA/CuCl<sub>2</sub> composites samples, i.e., red shifted. Also, at ~ 778.07 nm a localized surface plasmon

demonstrates the existence of interactions between electrons and photons in our samples. Increasing the values of optical dielectric constant of the PVA/CuCl<sub>2</sub> composite samples compared to pure PVA confirms the occurrence of more density of states (DOS), resulting in increased polarization that enhances the dielectric constant values [44]. The behavior of  $\epsilon'$  displays a wide dispersion region below 500 nm due to polar nature of PVA/CuCl<sub>2</sub> composite samples that follows the fluctuations of the incident electric field. This dispersion region plays a vital role in optical communication as well as in the design of optical devices. Higher values of imaginary part of optical dielectric constant ( $\epsilon''$ , optical loss), as shown in Fig. 8b, is attributed to the dipolar polarization [45].

resonance (LSPR) band has been observed in the visible range of the spectra of PVA/CuCl<sub>2</sub> composite samples. Pure PVA showed an indirect and direct optical energy gap of 4.71 and 5.08 eV, which decreased to 3.48 and 3.92 eV after incorporation of CuCl<sub>2</sub>, indicating a structural defect in the PVA matrix. The increase of Urbach energy with increasing CuCl<sub>2</sub> content confirmed the defects and imperfections in the semicrystalline structure of PVA. It was also observed that the values of  $\chi^{(1)}$ ,  $\chi^{(3)}$  and  $n_2$  for the composite samples are very high compared to pure PVA. These results could contribute to the development of PVA/CuCl<sub>2</sub> composites for using in optical sensors and optoelectronic devices. Also, the values of  $\epsilon'$  and  $\epsilon''$  are found to decrease with increasing the wavelength, while, the photoconductivity is increased with increasing the frequency.

### Acknowledgement

M. T. Ahmed and W. B. Elsharkawy thank Scientific Research Deanship (SRD) in Prince Sattam bin Abdulaziz University, KSA. Also, Z.M. Elqhtani thanks Deanship of Scientific Research (DSR) in Princess Nourah bint Abdulrahman University, Saudi Arabia for funding this research through the fast-track research funding program.

### Conflict of interest

There are no conflicts to declare.

## References

- [1] Tamgadge Y.S., Talwatkar S. S., Sunatkari, A. L., Pahurkar V.G., Muley G.G., Studies on nonlocal optical nonlinearity of Sr-CuO-polyvinyl alcohol nanocomposite thin films. *Thin Solid Films*, 595, 48–55 (2015). <https://doi.org/10.1016/j.tsf.2015.10.039>
- [2] Banerjee M., Sachdev P., Mukherjee G. S., *J. Appl. Phys.*, Preparation of PVA/Co/Ag film and evaluation of its magnetic and microstructural properties, 111, 094302 (2012). DOI: [10.1063/1.4708058](https://doi.org/10.1063/1.4708058)
- [3] Mukherjee G.S., *J. Therm. Anal. and Calorim.*, Calorimetric characterization of membrane materials based on polyvinyl alcohol, 96 (1), 21–25 (2009). <https://doi.org/10.1007/s10973-008-9833-1>
- [4] Devi C.U., Sharma A. K., Rao V.V.R.N., Electrical and optical properties of pure and silver nitrate-doped polyvinyl alcohol films, *Mat. Lett.*, 56, 167–174 (2002). [https://doi.org/10.1016/S0167-577X\(02\)00434-2](https://doi.org/10.1016/S0167-577X(02)00434-2)
- [5] Owolabi T. O., Rahman Mohd A. Abd., Modeling the Optical Properties of a Polyvinyl Alcohol-Based Composite Using a Particle Swarm Optimized Support Vector Regression Algorithm, *Polymers*, 13, 2697-16 (2021). <https://doi.org/10.3390/polym13162697>
- [6] Couture J.J., Lessard R.A., Modulation transfer function measurements for thin layers of azo dyes in PVA matrix used as an optical recording material. *Appl. Opt.*, 27, 3368–3374 (1988). <https://doi.org/10.1364/AO.27.003368>
- [7] Fahmy T., sarhan A., Elqahtani Z. M., Structural and Optical Characterization of Thiourea-Poly (Vinyl Alcohol) Composites, *Inter. J. of Eng. Res. & Techn.* 13(3), 454-461 (2020).
- [8] Fahmy T., Sarhan A., Elsayed I. A., Ahmed M. T., Effect of UV Irradiation on The Structure and Optical Properties of PVA/CuCl<sub>2</sub>, *J. of Advances in Physics*, 14(2), 5378-5387 (2018). <https://doi.org/10.24297/jap.v14i2.7358>
- [9] Fahmy T., Relaxation and Electrical Conductivity Study in Thiourea- Doped Poly (Vinyl Alcohol), *Intern. J. Polymeric Mater.*, 50, 109-127 (2001). <https://doi.org/10.1080/00914030108035094>
- [10] N. K. Subramani, S. Shivanna, S. K. Nagaraj, H. Siddaramaiah, Refractive index engineering of poly (vinyl alcohol)/Li<sub>2</sub>ZnO<sub>2</sub> nanocomposites: Effect of filler content and annealing temperature, *AIP Conference Proceedings* 1943, 020127 (2018). <https://doi.org/10.1063/1.5029703>
- [11] Prabha K., Jayanna H. S., Study the Frequency Dependence of Dielectric Properties of Gamma Irradiated PVA<sub>(1-x)</sub>PS<sub>x</sub> Polymer Blends, *Open J. Polym. Chem.* 5, 47e54 (2015). doi: [10.4236/ojpcem.2015.54006](https://doi.org/10.4236/ojpcem.2015.54006).
- [12] Saini I., Rozra J., Chandak N., Aggarwal S., Sharma P. K., Sharma A., Tailoring of electrical, optical and structural properties of PVA by addition of Ag nanoparticles. *Mater. Chem. Phys.*, 139, 802–810 (2013). <https://doi.org/10.1016/j.matchemphys.2013.02.035>
- [13] Shetty G., Crasta V., Kumar R., Rajesh K., Bairyd R., Patil P. S., Promising PVA/TiO<sub>2</sub>, CuO filled nanocomposites for electrical and third order nonlinear optical applications, *Optical Materials*, 95, (2019) 109218. <https://doi.org/10.1016/j.optmat.2019.109218>
- [14] Haroun A. A., Kamel S., Elnahrawy A. M., Hammad A. A., Hamadneh, I., Al-Dujaili A. H., Polyacetal/graphene/polypyrrole and cobalt nanoparticles electroconducting composites, *Inter. J. of Industrial Chem.*, 11, (2020) 223. <https://doi.org/10.1007/s40090-020-00218-w>
- [15] Abdel-Fattah E. , Alharthi A. I., Fahmy T., Spectroscopic, optical and thermal characterization of polyvinyl chloride-based plasma-functionalized MWCNTs composite thin films, *Applied Physics A.*, 125, (2019) 475. <https://doi.org/10.1007/s00339-019-2770-y>
- [16] Mahendia S., Tomar A.K., Kumar S., Nano-Ag doping induced changes in optical and electrical behaviour of PVA films, *Mater. Sci. Eng. B* 176, 530-534 (2011). <https://doi.org/10.1016/j.mseb.2011.01.008>
- [17] Kaur G., Verma R.K., Rai D. K., Rai S. B., Plasmon-enhanced luminescence of Sm complex using silver nanoparticles in Polyvinyl Alcohol, *J. Luminescence* 132, 1683-1687 (2012). <https://doi.org/10.1016/j.jlumin.2012.02.014>
- [18] Filippo E., Sera A., Manno D., Poly(vinyl alcohol) capped silver nanoparticles as localized surface plasmon resonance-based hydrogen peroxide sensor, *Sens. Actuators B Chem.*, 138, (2009) 625–630. DOI: [10.1016/j.snb.2009.02.056](https://doi.org/10.1016/j.snb.2009.02.056)
- [19] Guo L., Yang S., Yang C., Ping Y., Wang J., Ge W., Wong G. K.L., Highly monodisperse polymer-capped ZnO nanoparticles: Preparation and optical properties, *Appl. Phys. Lett.* 76, 2901-2903 (2000). <https://doi.org/10.1063/1.126511>
- [20] Vladimir A.E.B., Jose R.R.M., Nancy V.P.A., et al. In infrared spectroscopy-materials science, engineering and technology. UK: Intech Open; (2012). p. 195.
- [21] Wleczorek W., Stevens J.R., Impedance spectroscopy and phase structure of polyether–poly(methyl methacrylate)–LiCF<sub>3</sub>SO<sub>3</sub> Blend-Based Electrolytes. *Phys. Chem. B.*, 191 1529–1534 (1997). <https://doi.org/10.1021/jp962517w>
- [22] Wang H., Fang P., Chen Z., Wang S., Synthesis and characterization of CdS/PVA nanocomposite films. *Appl. Surf. Sci.*, 253(1) 8495–8499 (2007). DOI: [10.1016/j.apsusc.2007.04.020](https://doi.org/10.1016/j.apsusc.2007.04.020)
- [23] Baran E. J., Wagner C. C., Torre M. H., Kremer E., Kwerler P., Vibrational Spectra of the Cu(II) Complexes of Aspartic and Glutamic Acids, *Acta Farm. Bonaerense* 19 (3): 231-4 (2000).
- [24] Kiran K. K., Ravi M., Pavani Y., Bhavani S., Sharma A.K., Narasimharao V.V.R. Investigations on PEO/PVP/NaBr complexed polymer blend electrolytes for electrochemical cell applications.

- Memb Sci., 454 200–211 (2014). DOI: [10.1016/j.memsci.2013.12.022](https://doi.org/10.1016/j.memsci.2013.12.022)
- [25] Pandey M., Joshi G.M., Deshmukh K., Khutia M., Ghosh N.N., Optimized AC conductivity correlated to structure, morphology and thermal properties of PVDF/PVA/Naf ion composites, *Ionics*, 20(10) 1111-6 (2014). DOI: [10.1007/s11581-014-1111-6](https://doi.org/10.1007/s11581-014-1111-6)
- [26] Saion E., Susilawati, Doyan A., Abidin S. Z., Azmi Z., Zulkfli A., Zaki A. R. M., Dahlan K. Z. H., Karni T., Changes in the optical band gap and absorption edge for gamma-irradiated polymer blends, *J. Appl. Sci.*, 5(10) 1825-1829 (2005). DOI: [10.3923/jas.2005.1825.1829](https://doi.org/10.3923/jas.2005.1825.1829)
- [27] Choudhary S., Characterization of amorphous silica nanofiller effect on the structural, morphological, optical, thermal, dielectric and electrical properties of PVA–PVP blend based polymer nanocomposites for their flexible nanodielectric applications, *J. Mater. Sci. Mater. Electron.* 29, 10517-10534 (2018). <https://doi.org/10.1007/s10854-018-9116-y>
- [28] Pardey A. J., Rojas A. D., Y´anez J. E., Betancourt P., Scott C., Urbina C., Moronta D., Longo C., Spectroscopic characterization of coordination complexes based on dichlorocopper(II) and poly(4-vinylpyridine): Application in catalysis, *Polyhedron* 24, 511-519 (2005). <https://doi.org/10.1016/j.poly.2004.12.014>
- [29] Ghosh S. K., Pal T., Interparticle Coupling Effect on the Surface Plasmon Resonance of Gold Nanoparticles: From Theory to Applications, *Chemical Reviews* 107, 4797-4862 (2007). <https://doi.org/10.1021/cr0680282>
- [30] Urbach F., The Long-Wavelength Edge of Photographic Sensitivity and of the Electronic Absorption of Solids, *Phys. Rev.* 92, 1324 (1953). DOI: <https://doi.org/10.1103/PhysRev.92.1324>
- [31] Fahmy T., Sarhan A., Characterization and molecular dynamic studies of chitosan–iron complexes, *Bull. Mater. Sci.*, 44, 142-12 (2021). <https://doi.org/10.1007/s12034-021-02434-1>
- [32] Fahmy T., Sarhan A., Elsayed I. A., Abdelwahed H. G., Optical Properties of Poly(Vinyl Chloride-co-Vinyl Acetate-co-2-Hydroxypropyl Acrylate)/(Acrylonitrile-Butadiene-Styrene) Blends, *Inter. J. of Eng., Research &Tech.*, 11(9), 1405-1415 (2018).
- [33] Tauc J., Mentha A., Wood D., Optical and Magnetic Investigations of the Localized States in Semiconducting Glasses, *Phys. Rev. Lett.* 25, 749-752 (1970). <https://doi.org/10.1103/PhysRevLett.25.749>
- [34] Soliman T. S., Vshivkov S. A., Effect of Fe nanoparticles on the structure and optical properties of polyvinyl alcohol nanocomposite films, *J. Non-Cryst. Solids*, 519, 119452 (2019). <https://doi.org/10.1016/j.jnoncrysol.2019.05.028>
- [35] Fink D., Chung W. H., Klett R., Schmoltd A., Cardoso J., Montiel R., Vazquez, L. Wang M. H., Hosoi F., Omichi H., Langer P. G., Carbonaceous clusters in irradiated polymers as revealed by UV-Vis spectrometry, *Radiat. Eff. Def. Solids* 133, 193-208 (1995). <https://doi.org/10.1080/10420159508223990>
- [36] Chahal R. P., Mahendia S., Tomar A. K., Kumar S.,  $\gamma$ -Irradiated PVA/Ag nanocomposite films: Materials for optical applications, *J. of Alloys and Compounds* 538, 212-219 (2012). <https://doi.org/10.1016/j.jallcom.2012.05.085>
- [37] Wemple S. H., DiDomenico Jr. M., Behavior of the Electronic Dielectric Constant in Covalent and Ionic Materials, *Phys. Rev. B* 3, 1338-1351 (1971). <https://doi.org/10.1103/PhysRevB.3.1338>
- [38] Ali F.M., Structural and optical characterization of [(PVA:PVP)-Cu<sup>2+</sup>] composite films for promising semiconducting polymer devices, *J. Mol. Struct.*, 1189, 352-359 (2019). <https://doi.org/10.1016/j.molstruc.2019.04.014>
- [39] Soliman T.S., Vshivkov S.A., Elkalashy Sh.I., Structural, linear and nonlinear optical properties of Ni nanoparticles– Polyvinyl alcohol nanocomposite films for optoelectronic applications, *Optical Materials* 107, 110037 (2020). [10.1016/j.optmat.2020.110037](https://doi.org/10.1016/j.optmat.2020.110037)
- [40] Khoshman J. M., Hilfiker J. N., Tabet N., Kordesch M. E., Multiple oscillator models for the optical constants of polycrystalline zinc oxide thin films over a wide wavelength range, *Appl. Surf. Sci.*, 307, 558-565 (2014). <https://doi.org/10.1016/j.apsusc.2014.04.073>
- [41] Cotter D., Manning R., Blow K., Ellis A., Kelly A., Nessel D., Phillips I., Poustie A., Rogers D., Nonlinear Optics for High-Speed Digital Information Processing, *Science* 286, 1523-1528 (1999). DOI: [10.1126/science.286.5444.1523](https://doi.org/10.1126/science.286.5444.1523)
- [42] Tichý L., Ticha H., Nagels P., Callaerts R., Mertens R., Vlček M., Optical properties of amorphous As–Se and Ge–As–Se thin films, *Mater. Lett.* 39, 122-128 (1999). [https://doi.org/10.1016/S0167-577X\(98\)00227-4](https://doi.org/10.1016/S0167-577X(98)00227-4)
- [43] Tichá H., Tichý L., Semiempirical relation between non-linear susceptibility (refractive index), linear refractive index and optical gap and its application to amorphous chalcogenides, *J. Optoelectron. Adv. Mater.* 4(2), 381-386 (2002).
- [44] Fahmy T., Ahmed M. T., El-kotp A., Abdelwahed H. G., Alshaeer M. Y., Broadband Dielectric Spectroscopy and Electric Modulus Analysis of Poly (3-hydroxybutyrate-co-3-hydroxyvalerate) and Related Copolymers Films, *Inter. J. of Phys. & Appl.*, 8(1), 1-14, (2016).
- [45] Aslam M., Kalyar M. A., Raza Z. A., Graphene oxides nanosheets mediation of poly(vinyl alcohol) films in tuning their structural and opto-mechanical attributes, *J. Mater. Sci: Mater Electron.*, 28, 13401-13413 (2017). <https://doi.org/10.1007/s10854-017-7177-y>
- [46] Fahmy T., Elzanaty H., AC Conductivity and Broadband Dielectric Spectroscopy of Poly (Vinyl Chloride)/ Poly (Ethyl Methacrylate) polymer blend, *Bulletin of Mater. Sci.*, 42, 220 (2019). <https://doi.org/10.1007/s12034-019-1906-1>
- [47] Fahmy T., Elhendawi H., Elsharkawy W. B., Reicha F. M., AC conductivity and dielectric relaxation of chitosan/poly(vinyl alcohol) biopolymer polyblend, *Bull Mater Sci.*, 43, 243 (2020). DOI: [10.1007/s12034-020-02207-2](https://doi.org/10.1007/s12034-020-02207-2)